frontiers | Frontiers in Energy Research

TYPE Original Research
PUBLISHED 20 August 2025
DOI 10.3389/fenrg.2025.1654095

OPEN ACCESS

EDITED BY
Athanasios I. Papadopoulos,
Centre for Research and Technology Hellas (CERTH), Greece

REVIEWED BY
Solmaz Nadiri,
Physical-Technical Federal Institute, Germany
Vinay Kumar V.,
National Institute of Technology, India

*CORRESPONDENCE
Signe Kjelstrup,
signe.kjelstrup@ntnu.no

RECEIVED 25 June 2025
ACCEPTED 30 July 2025
PUBLISHED 20 August 2025

CITATION
Mendoza DF, Quintero-Díaz JC and Kjelstrup S (2025) Entropy production minimization in a tubular ammonia synthesis reactor: a mathematical optimization approach with variable geometry and heat flux control.
Front. Energy Res. 13:1654095.
doi: 10.3389/fenrg.2025.1654095

Entropy production minimization in a tubular ammonia synthesis reactor: a mathematical optimization approach with variable geometry and heat flux control

Diego F. Mendoza[1], Juan Carlos Quintero-Díaz[1] and Signe Kjelstrup[2]*

[1]Department of Chemical Engineering, Universidad de Antioquia, Medellín, Colombia, [2]PoreLab, Department of Chemistry, Norwegian University of Science and Technology, NTNU, Trondheim, Norway

Ammonia is one of the most widely produced chemicals worldwide and is increasingly considered a promising hydrogen carrier for energy storage. We propose a novel thermodynamic optimization strategy for tubular ammonia reactors based on second-law analysis and variable reactor geometry. Assuming thermal performance is already maximized through heat exchange, we explore how variations in reactor radius can further minimize entropy generation. Our steady-state mathematical model shows that geometry optimization alone can reduce total entropy production by 57% and pressure drop by 96%, without affecting ammonia yield or catalyst usage. Sensitivity analysis highlights the role of thermal boundary conditions on reactor performance. This study demonstrates that integrating geometric design with entropy minimization principles can significantly enhance the thermodynamic efficiency and sustainability of industrial chemical reactors.

KEYWORDS

entropy production, ammonia reactor, Haber-bosch process, heat transfer, geometric design

1 Introduction

Ammonia is one of the most important chemicals in industry due to its widespread use in the production of fertilizers, explosives, synthetic fibers, and more recently as a carbon-free energy carrier (Kojima and Yamaguchi, 2022). It is considered an efficient hydrogen carrier, offering a higher hydrogen density per unit volume than liquid hydrogen. This characteristic facilitates its storage and transportation, as ammonia can be stored under moderate pressure and temperature conditions compared to hydrogen (Chai et al., 2021; Meriño et al., 2025).

Ammonia production is energy intensive (30 GJ/ton NH_3), consuming about 2% of world's total energy production and generating 1%–2% of the anthropogenic CO_2 emissions worldwide (2.16 ton CO_2 per ton NH_3) (IEA, 2021; Ghavam et al., 2021;

Ye and Tsang, 2023). At industrial scale, ammonia production is typically carried out using the Haber-Bosch process where ammonia is synthesized from nitrogen and hydrogen at high pressures (15–30 MPa) in presence of cobalt-molybdenum nitride, iron- or ruthenium-based catalysts (Liu, 2014; El-Shafie and Kambara, 2023). Nitrogen is typically obtained from air, while hydrogen comes from hydrocarbons such as methane (Riera et al., 2023).

One of the main concerns is how to produce more ammonia to meet its increasing demand while diminishing the emissions (IEA, 2021). This requires encompassing policies and technologies to promote near-zero-emission production methods, such as using water instead methane as hydrogen source, generating small-scale decentralized production plants, as well as increasing the energy efficiency of the process (Ghavam et al., 2021; Smith et al., 2020; Amhamed et al., 2022; Ojelade et al., 2023; Erfani et al., 2024).

Second law analysis, based on either exergy or entropy generation, is a well-established methodology for improving energy efficiency in chemical processes, including reactor systems (Kumar and Sharma, 2025; Flórez-Orrego and de Oliveira Junior, 2017b; Penkuhn and Tsatsaronis, 2017; Flórez-Orrego and de Oliveira Junior, 2017a; Johannessen and Kjelstrup, 2004; Bedeaux et al., 1999). In this framework, an efficient process is one that minimizes entropy production, reflecting lower irreversible losses and improved exergy utilization. Despite its potential, second law efficiency is not yet systematically applied in the design and optimization of chemical reactors (Kjelstrup et al., 2010). Nonequilibrium thermodynamics provides a direct theoretical link to this approach through the concept of entropy production. Consequently, the entropy balance of the process becomes a fundamental tool. In light of current concerns regarding energy savings and storage, we are motivated to contribute to a more systematic integration of second law principles. In particular, we emphasize the importance of giving the entropy balance equation a more prominent role in the energy accounting of chemical processes.

In the Haber-Bosch process, exergy losses largely stem from heat exchange within the reactor and during ammonia recovery, accounting for 52%–65% of the total. Meanwhile, pressure drop in the reactor contributes about 5% to the overall entropy production within the reactor (Kirova-Yordanova, 2004). Moreover, the reactor type and its operating pressure profoundly influence the efficiency of the ammonia synthesis loop. This choice directly impacts the exergy destruction linked to both heat integration and the introduction of the feed gas (Penkuhn and Tsatsaronis, 2017).

Optimization of ammonia reactors have focused on finding the best multi-bed adiabatic reactors with intercooling (Flórez-Orrego and de Oliveira Junior, 2017b; Cheema and Krewer, 2019; Farsi et al., 2021) and on finding temperature profiles along the reactors that maximize ammonia conversion by manipulating thermal load (Månson and Andresen, 1986). Works on entropy production analysis in ammonia reactors have also analyzed multi-bed adiabatic reactors with intercooling as well as non-adiabatic reactors. It has been found that the inlet flow rate in multi-bed reactors gives rise to a dramatic increase in the entropy production (Xie et al., 2022). The irreversibilities were associated with chemical reaction and pressure drop, while the nitrogen-hydrogen ratio had a rather small influence on the entropy production.

Nummedal et al. (2003) minimized the entropy production of ammonia reactors with external cooling for different heat transfer coefficients, U, by manipulating the cooling media profile. They achieved reductions in entropy production from 3.9% ($U = 100$ W/K m^2) to 16% ($U = 400$ W/K m^2) with respect to the reference case where the inlet temperature of the cooling media was the manipulated variable. Several reactor optimization studies have found numerical evidence for a more uniform distribution of entropy production under optimal conditions (Sauar et al., 1999; Johannessen and Kjelstrup, 2004). In special cases, there is even equipartition of entropy production (Kjelstrup et al., 2010; Santoro et al., 2024).

The studies conducted by Månson and Andresen (1986), together with those by Nummedal et al. (2003) shall provide this work with a convenient point of reference, a Base Case. Our modelling results shall be compared at similar conditions with these results from the literature. We shall next proceed to assume that all necessary cooling is available at the temperature dictated by the Base Case. This provides us with an ideal reference case, ideal in the sense that the temperature profile is derived from a condition of maximum ammonia produced. This choice is reasonable, given that a study of the effect of heat transfer was done already by Nummedal et al. (2003).

In this contribution we assume that the cooling is available at the temperature dictated by the Base Case. For the influence of the heat transfer in the entropy production in ammonia reactor we refer the reader to the work of Nummedal et al. (2003).

High fidelity mathematical models and advanced manufacturing processes, such as 3D printing, have enabled shape optimization in chemical reactor design (Begall et al., 2023). This tool allows finding geometries that optimize performance criteria while satisfying process and manufacturing constraints (Courtais et al., 2021; Courtais et al., 2023). The simplest shape optimization methods include a set of geometric parameters, such as length, radii and angles, as decision variables in the optimization (Chen et al., 2007). Second Law analysis including shape optimization have been applied to SO_2 synthesis in tubular reactors using reactor radius as decision variable (Kizilova et al., 2024; Magnanelli et al., 2019). In the case studied by Magnanelli et al. (2019) it was found that shape optimization reduced the entropy production by 16% with respect to the optimized, constant-radius tubular reactor. Such a significant reduction in entropy production can lead to more sustainable chemical processes. In the case of ammonia synthesis reactors, shape optimization could also play a key role together with catalyst design, green hydrogen sources and process integration to achieve sustainable ammonia production. To the best of our knowledge studies are lacking reactor shape and entropy production in the ammonia synthesis process.

In this work we find the temperature profile and geometry (length and radius distribution) that minimizes the entropy production of a packed-bed tubular reactor and compare it with the optimal Base Case design of a tubular reactor with constant diameter. In both cases the designs use the same amount of catalyst and obtain a product with the same ammonia composition and flow.

10.3389/fenrg.2025.1654095

TABLE 1 Kinetic parameters (Nielsen et al., 1964).

Parameter	Units	Value
K_{b0}	mol NH_3 atm/(m^3 s)	2.19×10^{10}
$E_{a,b}$	kJ/mol	46.752
$K_{c,0}$	$atm^{1/2}$	2.94×10^{-4}
$E_{a,c}$	kJ/mol	100.66
α	–	0.6

TABLE 2 Beattie-Bridgman parameters (Månson and Andresen, 1986).

Species	A_i	B_i	C_i
	(J m^3/mol^2)	(m^3/mol)	(K^3 m^3/mol)
H_2	20.01×10^{-3}	20.96×10^{-6}	0.504
N_2	136.23×10^{-3}	50.46×10^{-6}	42.0
NH_3	242.47×10^{-3}	34.15×10^{-6}	4768.7
Ar	130.78×10^{-3}	39.31×10^{-6}	59.9
CH_4	230.70×10^{-3}	55.87×10^{-6}	128.3

2 Methodology

2.1 Physical-chemical model

The model was derived for a steady-state, packed-bed tubular reactor with variable cross section area and is based on the work of Magnanelli et al. (2019). The main assumptions of the model are: (i) plug flow, (ii) negligible temperature difference between gas bulk and catalyst, and (iii) validity of Ergun's equation to compute pressure drop.

In a control volume $\pi r^2 dl$ along the reactor axis the mass balance is:

$$\frac{dy_i \dot{n}}{dl} = \nu_i \mathcal{R} \pi r^2 \tag{1}$$

$$\frac{d\dot{n}}{dl} = \sum_{k \in i} \nu_k \mathcal{R} \pi r^2 \tag{2}$$

where y_i is the mole fraction of species $i = \{H_2, N_2, NH_3, Ar, CH_4\}$, $\dot{n}$ is the total mole flow rate, r is the reactor radius, and ν_i is the stoichiometric coefficient of species i in the reaction:

$$1/2N_2 + 3/2H_2 \rightleftharpoons NH_3 \tag{3}$$

The reaction rate of ammonia formation, $\mathcal{R}$, is given by the expression (Nadiri et al., 2024):

$$\mathcal{R} = \frac{K_b}{K_c^{2\alpha}} \left[K_a^2 f_{N_2} \left(\frac{f_{H_2}^3}{f_{NH_3}^2} \right)^{\alpha} - \left(\frac{f_{NH_3}^2}{f_{H_2}^3} \right)^{1-\alpha} \right] \tag{4}$$

where α is the kinetic exponent ($0.5 \leq \alpha \leq 0.75$), K_b and K_c are kinetic coefficients, K_a is the thermodynamic equilibrium constant, and f_i the fugacity of species i in the mixture.

The kinetic coefficients, Equations 5 and 6, follow Arrhenius-type kinetic expressions (Nielsen et al., 1964):

$$K_b = K_{b0} \exp\left(-\frac{E_b}{RT} \right) \tag{5}$$

$$K_c = K_{c0} \exp\left(-\frac{E_c}{RT} \right) \tag{6}$$

where R is the ideal gas constant and T is the gas temperature. The values for the pre-exponential factors, K_{b0}, K_{c0}, and for the activation energies, E_b and E_c, are reported in Table 1.

The thermodynamic equilibrium constant, K_a is calculated as a function of temperature following the expression (Gillespie and Beattie, 1930):

$$\log K_a = -2.691122 \log T - 5.519265 \times 10^{-5} T + 2.6899 + 1.848863 \times 10^{-7} T^2 + \frac{2001.6}{T} \tag{7}$$

The fugacity of the species i in the gas mixture at temperature, T, pressure, p, and composition, y (mole fraction), is calculated as the product of the fugacity coefficient, ϕ_i and the pressure of i in the mixture,

$$f_i(T,p,y) = \phi_i(T,p,y)\, y_i p \tag{8}$$

The fugacity coefficient ϕ_i is derived from the Beatty-Bridgeman equation of state (Månson and Andresen, 1986):

$$RT \ln \phi_i = \frac{(\beta_i + D_i)}{RT} p \tag{9}$$

where β_i and D_i terms are calculated according to the expressions:

$$\beta_i = RTB_i - A_i R \frac{C_i}{T^2} \tag{10}$$

and

$$D_i = \left(A_i^{1/2} - \sum_j y_j A_j^{1/2} \right)^2 + \frac{1}{T^2} \left(C_i^{1/2} - \sum_j y_j C_j^{1/2} \right)^2 - \frac{3}{4RT} \left(B_i^{1/3} - \sum_j y_j B_j^{1/3} \right) \left(B_i^{2/3} - \sum_j y_j B_j^{2/3} \right) \tag{11}$$

The values of parameters A_i, B_i and C_i are provided in Table 2.

The energy balance for a differential section of the reactor dl, neglecting potential and kinetic energy contributions, is the following:

$$\frac{d\dot{n}h}{dl} = J_q 2\pi r \mathcal{C} \tag{12}$$

where $\dot{n}$ is the total molar flow, h is the molar enthalpy of the mixture, J_q is the local heat flux, and $\mathcal{C}$ is the local curvature of the heat transfer surface,

$$\mathcal{C} = \sqrt{1 + \mathcal{U}^2} \tag{13}$$

where $\mathcal{U}$ represents the local radius variation in the reactor,

$$\frac{dr}{dl} = \mathcal{U} \tag{14}$$

The enthalpy of the mixture is calculated using the residual approach:

$$h(T,p,y) = h^{IG}(T,y) + h^{R}(T,p,y) \tag{15}$$

The ideal gas contribution to enthalpy, h^{IG}, taking as reference state 298.15 K and 1 atm, is calculated from the standard enthalpy of formation, $\Delta H^0_{f,i}$ and the ideal gas heat capacity, C^0_{pi},

$$h^{IG}(T,y) = \sum_i y_i \left(\Delta H^0_{f,i} + \int_1^T C^0_{pi} dT \right) \tag{16}$$

The values for $\Delta H^0_{f,i}$ and C^0_{pi} are taken from the data base of Poling et al. (2001). The residual enthalpy of the mixture, h^R, is calculated from the Beatty-Bridgeman equation of state,

$$h^{R}(T,p,y) = \left[B_m - \frac{2A_m}{RT} - \frac{4C_m}{T^3} \right] p \tag{17}$$

where A_m, B_m and C_m are calculated from the following the mixing rules:

$$A_m = \left(\sum_i y_i A_i^{1/2} \right)^2 \tag{18}$$

$$B_m = \sum_i \sum_j y_i y_j \left(B_i^{1/3} + B_j^{1/3} \right)^3 \tag{19}$$

$$C_m = \left(\sum_i y_i C_i^{1/2} \right)^2 \tag{20}$$

where parameters A, B and C are reported in Table 2.

The local pressure drop is estimated from Ergun's equation,

$$\frac{dp}{dl} = -\left[150 \frac{\mu}{D_p^2} \frac{(1-\epsilon)^2}{\epsilon^3} + 1.75 \frac{\rho v}{D_p} \frac{(1-\epsilon)}{\epsilon^3} \right] v \tag{21}$$

where μ is the viscosity of the mixture, D_p is the catalytic pellet diameter, ϵ the void fraction, ρ, v are the gas density and velocity, respectively. The values of the parameters used in Equation 21 are given in Table 3.

The local gas flow velocity, v, is obtained using Equation 22:

$$v = \frac{\dot{m}}{\rho \pi r^2} \tag{22}$$

where $\dot{m}$ is the gas mass flow rate, r is the reactor radius, and ρ is the density of the mixture calculated from Equation 23:

$$\rho = \frac{p}{zRT} \tag{23}$$

The compressibility factor, z, is obtained from the Beattie-Bridgeman equation of state, Equations 24, 25:

$$z = 1 + \frac{\beta_m}{(RT)^2} p \tag{24}$$

and

$$\beta_m = RTB_m - A_m - \frac{RC_m}{T^2} \tag{25}$$

where A_m, B_m and C_m are calculated from the mixing rules presented in Equation 18.

2.2 Entropy production

The entropy production in the reactor, $(dS/dt)_{irr}$, is the integral of the local entropy production per unit length, σ', along the reactor length, Equation 26

$$\left(\frac{dS}{dt} \right)_{irr} = \int_0^l \sigma' \, dl \tag{26}$$

The local entropy production per unit length, Equation 27 is obtained using irreversible thermodynamics as the product of fluxes and thermodynamic forces (Kjelstrup et al., 2010),

$$\sigma' = \left[\mathcal{R} \left(-\frac{\Delta G_r}{T} \right) + v \left(-\frac{1}{T} \frac{dp}{dl} \right) \right] \pi r^2 \tag{27}$$

The first term on the right-hand-side of Equation 27 is the reaction rate, $\mathcal{R}$, multiplied by minus the reaction Gibbs energy, ΔG_r, divided by the local temperature, T. The second term is the product of the local velocity of the gas, v, by the pressure drop per unit length, dp/dl, divided by the temperature.

The thermodynamic reaction force is calculated from Equation 28 (Nummedal et al., 2003):

$$-\frac{\Delta G_r}{T} = -R \ln \left(\frac{a_{\mathrm{NH_3}}}{a_{\mathrm{H_2}}^{3/2} a_{\mathrm{N_2}}^{1/2} K_a} \right) \tag{28}$$

where R is the ideal gas constant, a_i is the activity of species i, calculated as the fugacity of component i in the mixture, $f_i(T,p,y)$, divided by the reference pressure, $p_0 = 1$ atm, while the equilibrium constant, K_a, is calculated from Equation 7.

3 Reactor optimization

The objective of control theory, a domain in variational calculus, is to find the function that optimizes a functional, when the optimization is also subject to constraints (Nolasco et al., 2021; Biegler, 2010). Here, we shall use the method twice, first to establish a Base Case reactor, and second to minimize the total entropy production of that reactor. Constraints apply in both cases. The reactor yield is the outcome of an optimization in the Base Case, but a constraint in the second case.

3.1 Base case

As Base Case (BC) we have taken an ideal reactor of 10 m length with a constant radius of 0.1 m. By ideal we mean that the reactor has an optimal temperature profile that maximizes the mole fraction of the ammonia outlet, $y_{\mathrm{NH_3}}(L = 10\,m)$. This is a relevant choice, consistent with the purpose of chemical reactors; to produce chemicals. The maximum production of ammonia is found from the optimal local heat flux, J_q, at an inlet temperature of the reactive mixture, $T(l = 0)$. The optimization problem formulation, Equations 29–31, for this case is as follows:

$$\max_{J_q(l), T(l=0)} y_{\mathrm{NH_3}}(L = 10\,m) \tag{29}$$

s.t.

10.3389/fenrg.2025.1654095

Equations 1-22

$$T_{min} \leq T(l=0) \leq T_{max} \tag{30}$$

$$J_{q,min} \leq J_q(l) \leq J_{q,max} \tag{31}$$

where Equations 1–22 are equality constraints corresponding to the differential-algebraic system of the reactor model, including its entropy production. The lower and upper bounds for the inlet temperature and for heat flux were set to $T_{min} =$ 300 K, $T_{max} =$ 950 K, $J_{q,min} = -5$ MW/m^2, and $J_{q,max} = 5$ MW/m^2, respectively. The high heat flux constraint allows exploring optimal solutions beyond the current achievable limits in chemical reactor technology. Sensitivity of the BC to the heat flux constraint is addressed in Section 4.3.

3.2 Entropy production minimization

The variables of entropy production minimization problem include the radius change, reactor length, heat flux and gas inlet temperature. The model is reformulated in terms of a dimensionless length, $0 \leq l^* \leq 1$, such that the reactor length, l, is calculated as the product of the dimensionless length and the total reactor length, L_{tot}, Equation 32,

$$l = L_{tot}\, l^* \tag{32}$$

The differential operator, d/dl, applied to any variable in the model is reformulated as according to Equation 33:

$$\frac{d}{dl} = \frac{1}{L_{tot}} \frac{d}{dl^*} \tag{33}$$

Once these changes are introduced in the model, the optimization problem is formulated as according to Equations 34–41:

$$\min_{J_q(l^*),\mathcal{U}(l^*),L_{tot},T(l^*=0)} \int_0^1 \sigma' L_{tot}\, dl^* \tag{34}$$

s.t.

Scaled Equations 1-22

$$T_{min} \leq T(l^*=0) \leq T_{max} \tag{35}$$

$$J_{q,min} \leq J_q(l^*) \leq J_{q,max} \tag{36}$$

$$\mathcal{U}_{min} \leq \mathcal{U}(l^*) \leq \mathcal{U}_{max} \tag{37}$$

$$L_{min} \leq L_{tot} \leq L_{max} \tag{38}$$

$$r_{min} \leq r(l^*) \leq r_{max} \tag{39}$$

$$m_{cat}(l^*=1) \leq m_{cat,max} \tag{40}$$

$$y_{NH_3}(l^*=1) \leq y_{NH_3,\min} \tag{41}$$

The equality constraints apply to the scaled model equations using dimensionless length l^*. Equations 36–38 are path constraints corresponding to the optimization controls: heat flux, J_q, local radius change, $\mathcal{U}$, and total reactor length, L_{tot}. Equation 39 defines a lower and upper bound for the radius, while the terminal constraints given by Equations 40–41 ensure that the amount of catalyst be less or equal to the catalyst mass spent in the Base Case (BC), and that the ammonia mole fraction be at least equal to the one obtained in the BC. The upper and lower bounds for this optimization problem are shown in Table 4.

TABLE 3 Reactor parameters (Nummedal et al., 2003).

Parameter	Symbol	Unit	Value
Hydrogen inlet mole fraction	y_{H_2}		0.633
Nitrogen inlet mole fraction	y_{N_2}		0.211
Ammonia inlet mole fraction	y_{NH_3}		0.036
Argon inlet mole fraction	y_{Ar}		0.04
Methane inlet mole fraction	y_{CH_4}		0.08
Inlet flow rate	$\dot{n}_{in}$	mol/s	147.063
Inlet pressure	p_{in}	MPa	26.462
Catalyst density	ρ_{cat}	kg/m^3	2600
Catalyst void fraction	ϵ		0.65
Total mass of catalyst	m_{cat}	kg	290

TABLE 4 Bounds for the minimum entropy production optimization case.

Variable	Unit	Lower bound	Upper bound
$T(l^*=0)$	K	300	950
$J_q(l^*)$	MW/m^2	−5	5
$\mathcal{U}(l^*)$		−1	1
L_{tot}	m	0.01	20
$r(l^*)$	m	0.05	0.15
$m_{cat}(l^*=1)$	kg		290
$y_{NH3}(l^*=1)$		0.221	

3.3 Model implementation

The model was implemented in the optimization modeling language Pyomo (Bynum et al., 2021). The differential algebraic model was discretized using orthogonal collocation on finite elements using the pyomo. dae extension (Nicholson et al., 2017). In this case the discretization consisted of 200 finite elements with 3

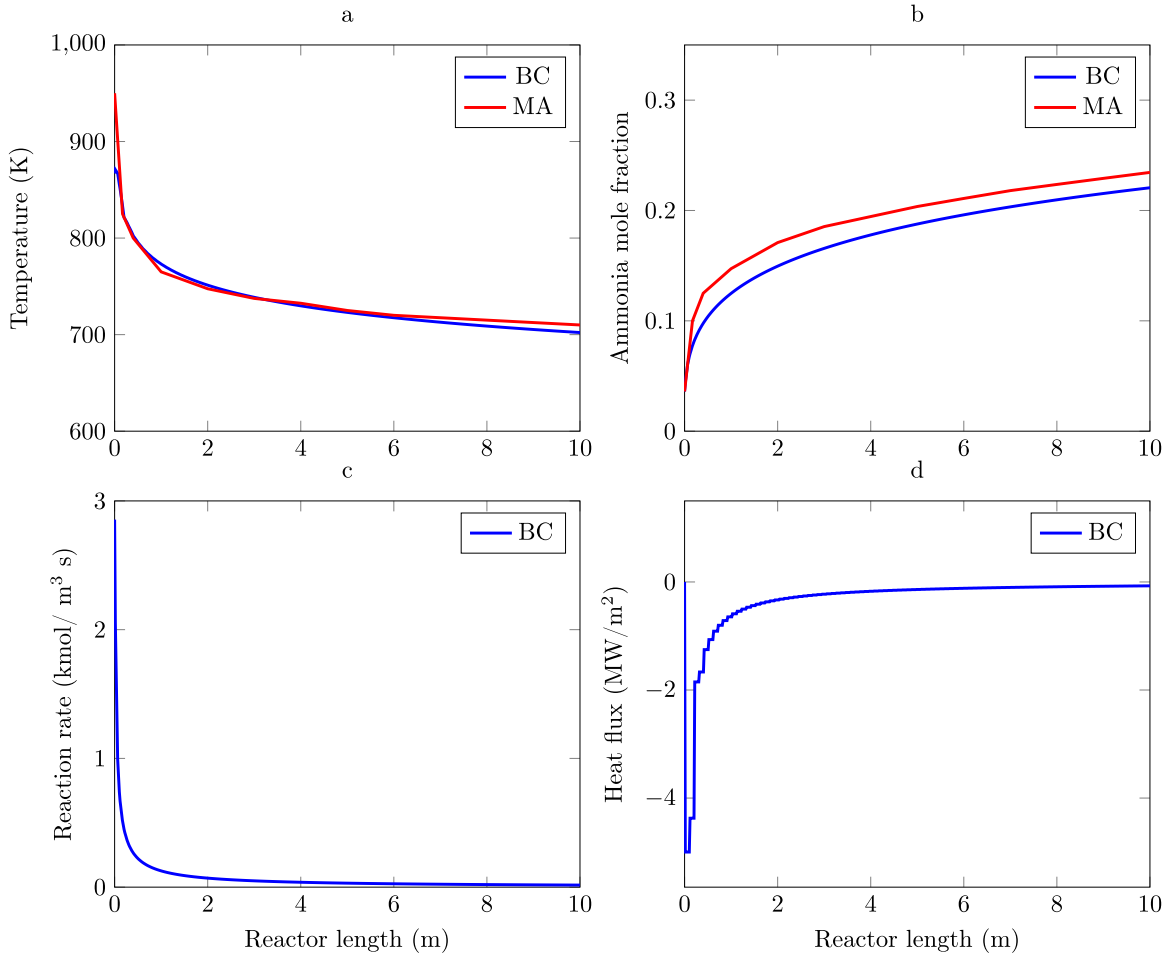

FIGURE 1
Ammonia production maximization for the Base Case (BC) and the work of Månson and Andresen (Månson and Andresen, 1986) (MA). **(a)** Temperature profile. **(b)** Ammonia mole fraction. **(c)** Reaction rate of ammonia production for BC. **(d)** Heat flux profile for BC.

Radau collocations points. The discretized model was solved in the large scale nonlinear optimization solver IPOPT 3.13.2.

4 Results and discussion

4.1 The base case

The Base Case (BC) is a reactor with maximum ammonia produced, given a heat flux and gas inlet temperature. The optimal gas temperature profile shown in Figure 1a implies a high inlet gas temperature (870 K) followed by cooling along the reactor. The main determinant of this behavior is the kinetic expression, Equation 4, which takes into account two antagonistic contributions: on one hand, the term $K_b/K_c^{2\alpha}$ increases with temperature, on the other hand, the equilibrium constant of the reaction, K_a, decreases as the temperature increases since the reaction is exothermic.

The reactor temperature profile (Figure 1a) is high at start (above 800 K) and declines sharply below 800K (Figure 1c). In the high temperature zone, the system is far from chemical equilibrium. The reaction rate experiences a very sharp decrease (Figure 1c). The high temperature zone corresponds to the first 0.5 m of the reactor (5% of the total reactor length) and is the most efficient reaction zone generating 40% of the total ammonia produced in the reactor.

An important point not handled here is catalyst deactivation. In terms of catalyst utilization, the high-temperature zone (up to 0.5 m along the reactor length) produces 0.62 mol/s of ammonia per kilogram of catalyst, compared to 0.048 mol/s per kilogram in the low-temperature zone (beyond 0.5 m along the reactor). However, catalysts exposed to temperatures above 800 K can rapidly deactivate, while below this threshold, catalyst deactivation remains low (Liu, 2014; Chonggen et al., 2011). Under these conditions, 95% of the total catalyst mass contributes to 60% of the total ammonia production.

The optimized reactor produces 22.3 mol of ammonia per second (32.7 metric ton/day) with an effluent composed of 22.01 (mole %) ammonia (Figure 1b). This optimal ammonia mole fraction is close to the 23.45 (mole %) obtained by Månson and Andresen (1986) who optimized an ammonia synthesis reactor with similar inlet composition and pressure, but without taking into account the pressure drop. The main difference between our and their results lies in the higher gas inlet temperature of about 950 K,

which leads to a higher ammonia mole fraction profile. Nonetheless, the optimal temperature and ammonia profiles reported by Månson and Andresen (1986) are in good agreement with those obtained in this work (see Figures 1a,b). This makes it now interesting to move one more step, and see if the energy efficiency also can be improved in terms of having a smaller entropy production.

The total cooling load required to carry out the process is 2.14 MW. As much as 67.3% of it (1.44 MW) is transferred in the first 2 m of the reactor (Figure 1d), while the last 2 m represents only 4.6% (0.1 MW) of the total transfer. One reason for this behavior, in addition to the reaction rate and thermodynamic equilibrium considered in the beginning of this section, is that the control of the heat released by the reaction is mainly located in the first part of the reactor.

The total pressure drop for the Base Case was 0.432 MPa (Figure 2a), corresponding to 1.65% of the inlet pressure (26.462 MPa), this pressure drop is constant per reactor length (0.0432 MPa/m) due to slight variations in flow velocity, between 1.8 and 2.4 m/s, (Figure 2b). In practical terms a lower pressure drop has a positive effect on reactor performance since ammonia production is thermodynamically and kinetically favored by high pressures, additionally higher reactor outlet pressures reduce the cooling duty necessary to recover ammonia by condensation before recirculation of unconverted reactants which would reduce econmic cost.

4.2 Entropy production minimization

Entropy production minimization was carried out keeping the same ammonia production (22.3 mol/s) and composition (22.01% molar) as well as total mass of catalyst (290 kg), using local radius change $\mathcal{U}$, reactor length, L_{tot}, gas inlet temperature, $T(l^* = 0)$, and local heat flux, J_q, as controls.

The optimal geometry (Figure 2c) results in a reactor with a length of 2.9 m and a radius distribution that increases linearly from 0.14 m in the inlet to 0.22 m in the outlet. The geometry diminishes the pressure drop by 96% with respect to the Base Case. The main reason for this lies in the in gas velocity reduction which has a quadratic contribution to the pressure drop expression as given by Ergun's equation, Equation 21.

The gas inlet temperature in the reactor with minimum entropy production reactor is, however, 80 K higher than in the Base Case reactor (Figure 2d). Higher inlet temperatures increase the initial reaction rate of the minimum entropy production reactor followed by a steeper decrease than in the Base Case reactor (Figure 2e). Temperature profiles show that the length of hot reaction zone, $T \geq 800$ K, is the same in both cases (0.5 m); however, the temperature in the hot zone tends to be higher in the minimum entropy production reactor. Besides, the temperature in the cold zone of the reactor with minimum entropy production is lower than this zone in the Base Case reactor.

The heat load distribution (Figure 2f) in the Base Case and the in the minimum entropy production design follow similar patterns. In both cases the greatest heat load is located in the first part of the reactor. The total cooling load in the reactor with minimum entropy production (2.49 MW) is 16% greater than in the Base Case. The main differences in heat load is from the first 0.5 m to the end of the reactor length. A way of using the cooling heat to increase thermal efficiency in the process is by generating steam (Flórez-Orrego and de Oliveira Junior, 2017b), which could increase the thermal efficiency of the minimum entropy production reactor with respect to the BC reactor.

The entropy production in the Base Case is 0.139 kW/K where 0.102 kW/K, 73% of the total entropy production (Figure 3a), is due to the reaction term in the entropy production equation. The reactor with minimum entropy production, Figure 3b, reduces the total entropy production by 57% with respect to the Base Case. A salient aspect of the thermodynamically optimal reactor is that the contribution of the reaction and pressure terms in the entropy production is 57% and 99% lower with respect to the Base Case, leading to a reactor design where almost all the irreversibility is due to reaction, since this term represents 98% the total entropy production. These are significant changes.

It is interesting to note that the local entropy production profiles show that entropy production is more evenly distributed in the EM case (Figure 3d) than in the BC (Figure 3c). The result give some support to the principle of equipartition of entropy production which identifies systems with minimum entropy as those that distribute entropy production evenly throughout the system (Tondeur and Kvaalen, 1987). However, exact equipartition is not expected for constrained optimization.

The heat transfer and geometry controls used in the EM case concerned two key reaction aspects, viz, the reaction temperature and pressure. As previously discussed, the first part of the EM reactor, where most ammonia is produced, has a low pressure drop with respect to the BC. The higher pressure present in the EM thermodynamically favors the production of ammonia. Geometry optimization is key to reduce the compression work required for ammonia condensation once it leaves the reactor, and to increase the reaction performance.

4.3 Heat flux sensitivity analysis

In Section 4.1, it was assumed that the heat flux J_q could be freely adjusted to achieve optimal operating conditions. However, in practical applications, heat transfer is often limited by material and design constraints. Such limitations may significantly influence the reactor's thermodynamic performance by increasing entropy production. We propose that a reduced maximum heat flux hinders operation close to reversible conditions, thereby amplifying irreversibilities. Consequently, we expect that this will affect critical operational and design parameters such as the temperature profile, catalyst use, pressure drop, and reactor radius.

The heat flux bounds for the EM case were $-5 \leq J_q \leq 5$ MW/m^2. Now the effect of reducing the available heat flux on the entropy production is explored. To this end we define a variable Equation 42 κ_q such that:

$$\kappa_q = \frac{J_{q,max}}{5\,\mathrm{MW/m^2}} \tag{42}$$

From this expression we define variable lower and upper bounds of the J_q constraint in terms of κ_q, such that: $-5 \cdot \kappa_q \leq J_q \leq 5 \cdot \kappa_q$ MW/m^2.

The optimization problem given by Equations 36–38 is solved for each value of κ_q ($0.1 \leq \kappa_q \leq 1$) in the constraint related to the allowed heat flux, Equation 36.

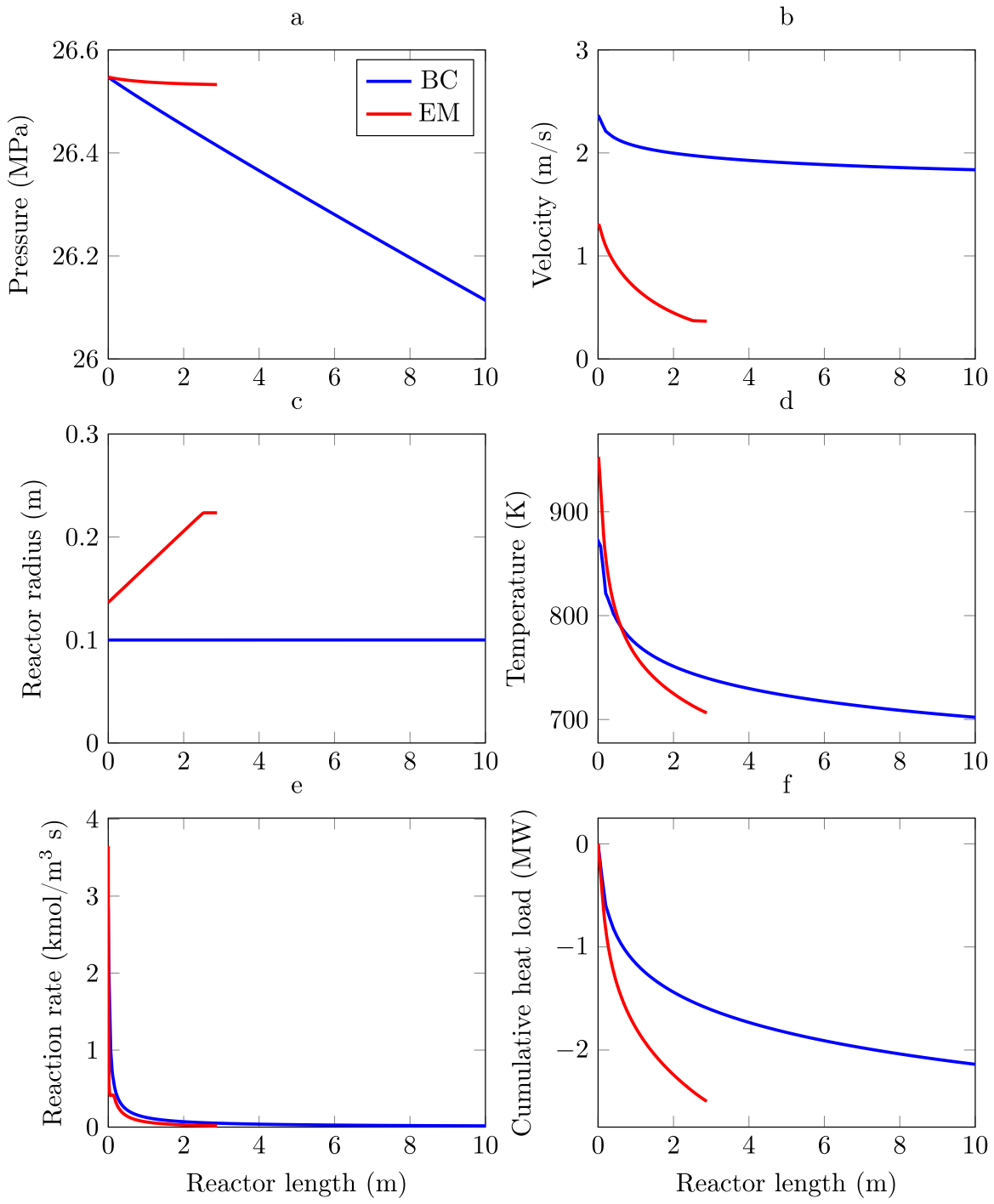

FIGURE 2
Profiles for the Base Case (blue curves) and the reactor with minimum entropy production (red curves). **(a)** Pressure. **(b)** Velocity. **(c)** Radius. **(d)** Temperature. **(e)** Reaction rate. **(f)** Cumulative heat load.

Figure 4a presents a Pareto front illustrating the relationship between the maximum allowable heat flux and the entropy production rate. It is observed that as the heat flux J_q decreases, the entropy production rate in the reactor increases. This suggests that a larger heat flux enables the reactor to operate in a more reversible manner, thereby reducing thermodynamic losses. When heat transfer is limited, the reactor experiences greater irreversibilities associated with chemical reaction and pressure drop. By examining Figure 4a, a point can be identified between the limits of 2 and 3 MW/m^2, beyond which, even with a higher heat flux allowed (e.g., up to 5 MW/m^2), the additional reduction in generated entropy is comparatively small. Moreover, increasing the system's maximum

10.3389/fenrg.2025.1654095

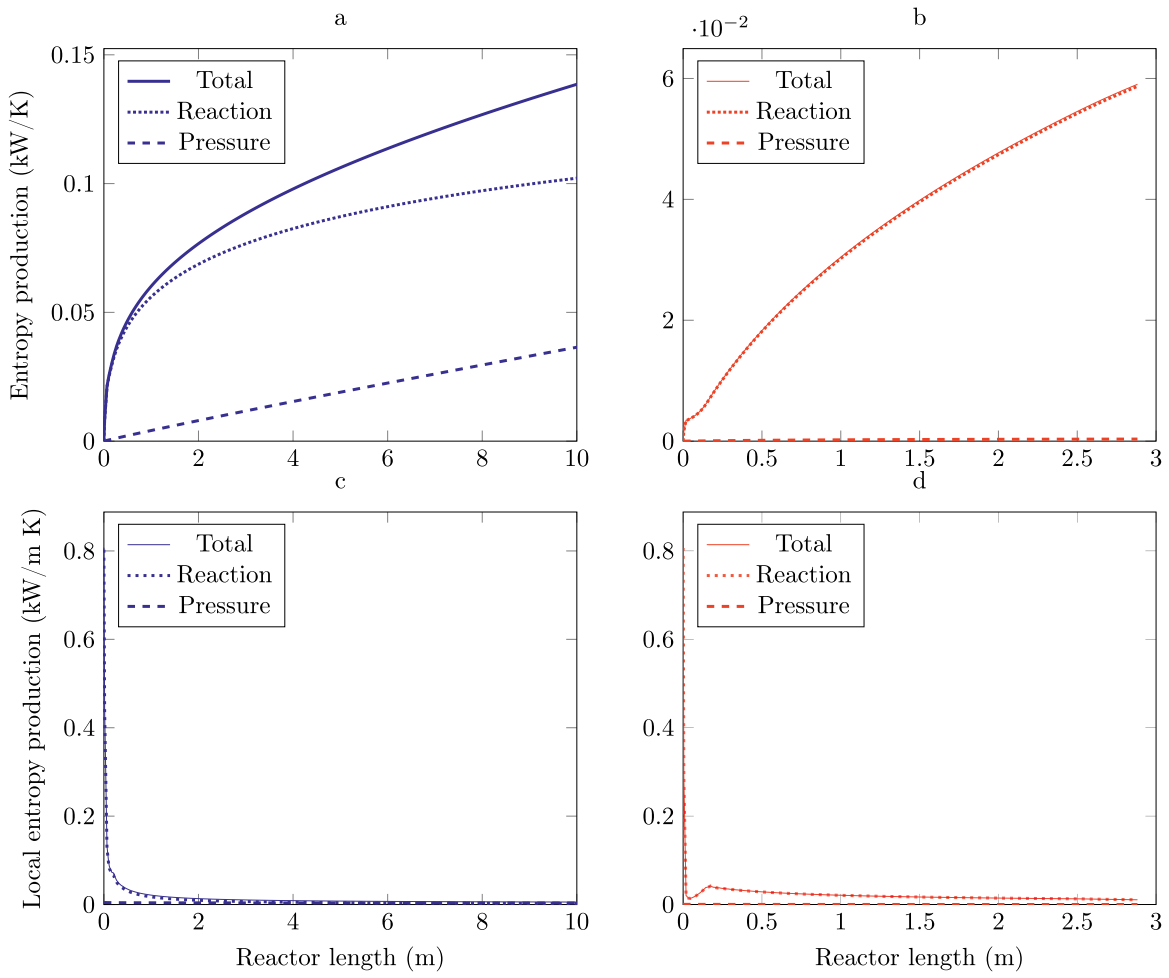

FIGURE 3
Entropy production profiles for the Base Case (blue lines) and the minimum entropy production reactor (red lines). **(a)** Cumulative entropy production BC. **(b)** Cumulative entropy production EM. **(c)** Local entropy production BC. **(d)** Local entropy production EM.

heat flux beyond this point may not be economically justifiable. From a practical perspective, it may be more feasible and cost-effective to design a cooling system that operates near the point of diminishing returns, around 0.5 MW/m^2 (Figure 4b). It is not necessary to oversize the cooling system beyond the point where the benefits in terms of entropy production reduction are marginal.

Figure 4b shows the heat flux profiles along the reactor for different values of $J_{q,max}$. For higher $J_{q,max}$ values, the heat flux profile exhibits more pronounced variations along the reactor, indicating the need for more intense heat transfer in the first part of the reactor to maintain the optimal temperature profile. As $J_{q,max}$ decreases, the heat flux profile becomes more uniform, and the absolute values of the heat flux are lower. Horizontal segments in some regions mean that the heat flux has reached its imposed upper or lower bound. Although the local heat fluxes are lower when heat transfer limitations are increased, to maintain the same conversion, the reactor length must be longer, as seen in Figure 4b. The total heat load removed will then be lower, as shown in Figure 4c.

As shown in Figure 4d, the gas temperature at the reactor inlet tends to decrease as the maximum allowed heat flux decreases. This occurs because, the optimization procedure aims to prevent an excessive increase in temperature in the initial section of the reactor, where the exothermic ammonia synthesis reaction is faster and releases a significant amount of heat with a lower heat removal capacity. By starting with a lower temperature, the heat generated along the reactor can be better managed under limited cooling capacity. This is consistent with observations showing that, toward the end of the reactor, temperatures tend to rise as the maximum heat flux decreases. The presence of "hot spots" in the temperature profile becomes more evident as the maximum allowed heat flux is reduced. This is because the limited capacity to remove the heat generated by the reaction leads to local accumulations of energy. When the reactor's cooling capacity is limited, it becomes impossible to maintain the optimal temperatures associated with higher heat flux, which prevents the minimization of entropy production. From a local perspective, to initiate the process at a lower temperature may reduce the entropy produced by the reaction; however, this also significantly lowers the reaction rate at the reactor inlet (Saffari et al., 2021). To achieve the same ammonia conversion under these conditions, the reactor would need to operate at higher temperatures

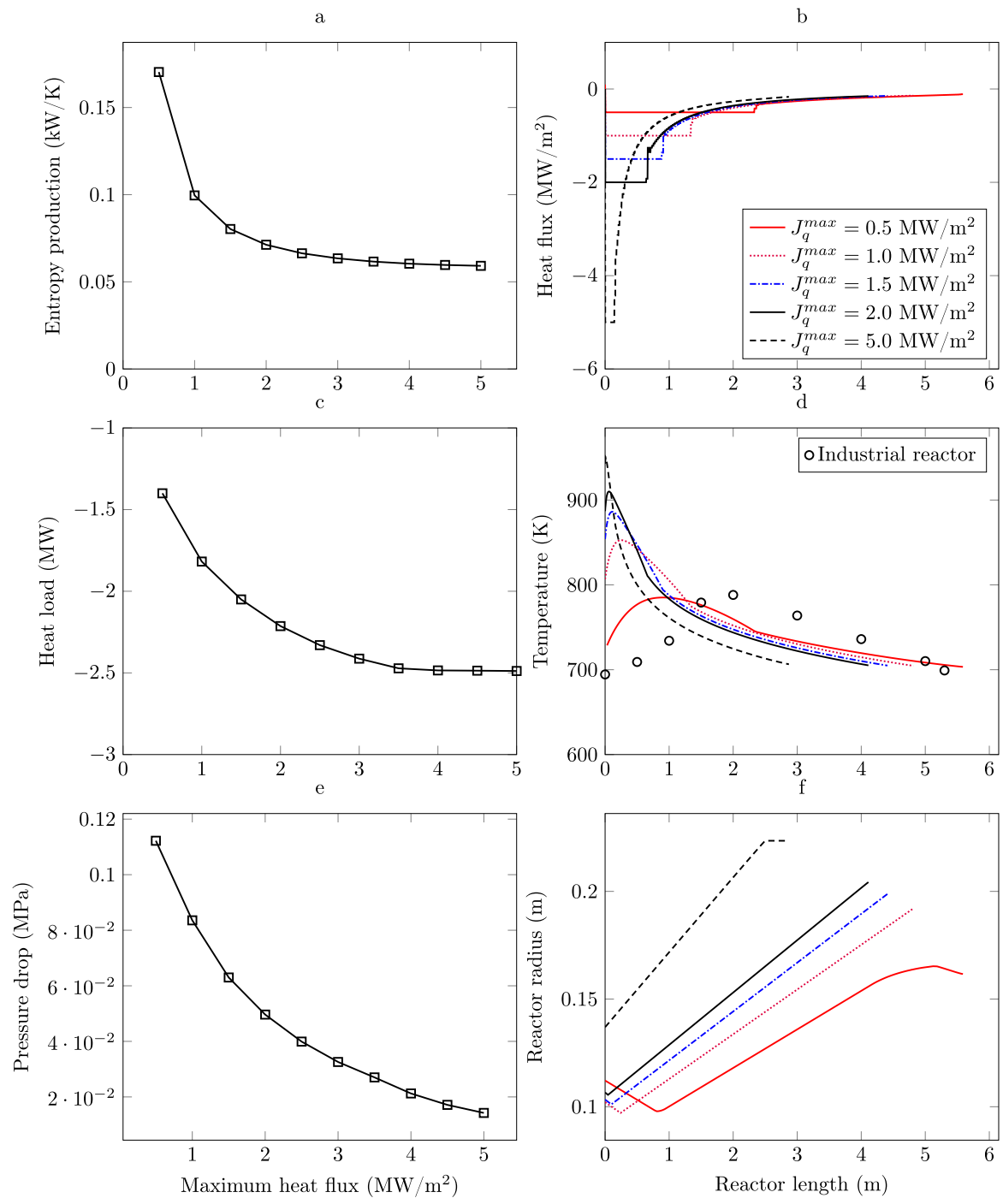

FIGURE 4
Heat flux sensitivity. **(a)** Entropy production rate Pareto front. **(b)** Heat flux profile. **(c)** Heat load vs. maximum heat flux constraint. **(d)** Optimal temperature profiles vs. maximum heat flux constraint. **(e)** Pressure drop vs. heat flux constraint. **(f)** Radius profile vs. heat flux constraint.

in other zones and may additionally require an increased length to compensate for the reduced thermal efficiency, resulting in greater overall entropy production.

To prevent catalyst deactivation, it is necessary to limit the temperature to 800 K, (Chonggen et al., 2011; Liu, 2014). It is observed that under low heat transfer constraints ($J_{q,max}$ between 5.0 and 1.0 MW/m^2), hot spots with temperatures exceeding 800 K appear in the initial sections of the reactor, covering between 15% and 25% of the reactor length. These conditions may limit reactor operation, at least until new developments in thermally more stable catalysts are achieved. However, the thermal profile obtained under the highest heat transfer restriction that is ($J_{q,max}$ = 0.5 MW/m^2) exhibits satisfactory temperature levels that allow the use of existing catalysts and also enable the implementation of standard heat

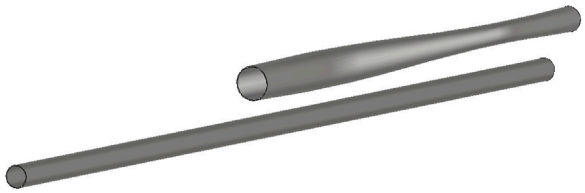

FIGURE 5
Ammonia reactor. Base Case geometry ($J_{q,max}$ = 5 MW/m^2) vs. EM optimized geometry ($J_{q,max}$ = 0.5 MW/m^2).

exchange systems. This profile is similar to those observed under industrial conditions in reactors with integrated heat exchange, represented by circle black markers in Figure 4d (Baddour et al., 1965). Under these heat transfer conditions, the entropy production is 0.17 kW/K, which is close to the value found for the Base Case (0.14 kW/K, Figure 3a). However, for the Base Case, the required heat transfer rate is 5.0 MW/m^2, which prevents its implementation using conventional heat transfer systems.

Figure 4e illustrates the relationship between pressure drop across the reactor and the maximum allowable heat flux for different design constraints. It is evident that as the maximum heat flux increases, the pressure drop across the reactor tends to decrease, leading to lower energy losses due to pressure drop and thereby minimizing this source of irreversibility. This reduction in pressure drop is achieved at the expense of an increase in reactor diameter, as shown in Figure 4f. The trend observed in Figure 4f suggests that when higher maximum heat flux per unit area is allowed (i.e., higher $J_{q,max}$), the optimal reactor design favors a geometry with a larger radius along its length. Conversely, when heat transfer is more restricted, the reactor radius decreases. Under these conditions, heat transfer is maximized through an increase in the lateral surface area-to-volume ratio (Mahapatra and Dasappa, 2014). This phenomenon also explains the marked reduction in the reactor diameter in the initial sections, followed by an increase in diameter toward the middle and end of the reactor. Since hot spots occur in these regions, a reduction in diameter enhances the heat transfer area per unit volume, thereby compensating for the limitations imposed on heat transfer. For the simulated capacity of 32.7 metric ton/day, this configuration features (Figure 4f line red) a variable-radius reactor geometry and a temperature profile below 800 K, ensuring catalyst stability.

As observed, a tubular reactor with constant radius (Base Case) results in high entropy production (0.14 kW/K), whereas a reactor with a monotonically increasing variable radius, achieving the same ammonia production and operating under the same allowable heat flux (5 MW/m^2), produces approximately 0.06 kW/K (only 43% of the entropy production with respect to the Base Case). However, this heat flux is excessive for current heat transfer systems. Therefore, a more realistic design, corresponding to a maximum heat flux of 0.5 MW/m^2, leads to a geometry like the one shown in Figure 4f (red line) and Figure 5, with an entropy production of 0.17 kW/K, similar to that of a tubular reactor operating at 5 MW/m^2 maximum heat flux.

From a mechanical design perspective, variations in radius along the reactor axis, especially if pronounced, would lead to a non-uniform distribution of stresses along the reactor walls due to internal pressure. To withstand these variable stresses and the high operating pressures, high-strength materials would be necessary, along with more sophisticated manufacturing processes, such as additive manufacturing (3D printing), instead of using a simple constant-radius tube. This would require further detailed studies, both at the simulation level and through experimental prototypes.

It is well known in chemical engineering that more reversible conditions can be approached by increasing the contact area for heat exchange. Similar systematic studies on decrease in the entropy production of the chemical reactor with varying geometric variables, has not been done. That geometric variables are important is, however, beyond doubt. This opens up for new important applications of our well-proven engineering mathematical procedures.

5 Conclusions and perspectives

In this work the entropy production minimization of a tubular chemical reactor for ammonia synthesis was carried out employing gas inlet temperature, heat flux and radius variation along the reactor length as control variables. The same amount of catalyst, maximum heat flux, and ammonia production was used in a tubular base case reactor yielding maximum ammonia production.

The results indicate that an optimized reactor design with a variable-radius profile and temperature control *via* heat flux can achieve a 96% reduction in pressure drop and a 57% decrease in total entropy production with respect to the tubular reactor.

A sensitivity analysis enabled the identification of an optimal design with minimum entropy production, suitable for practical implementation. The optimal design has variable-radius geometry and a temperature profile below 800 K, ensuring catalyst stability. It achieves a 70% reduction in pressure drop compared to the base-case reactor and a maximum heat flux of 0.5 MW/m^2, attainable with a heat transfer coefficient of 400 W/K.m^2·

Future work may focus on evaluating the plug flow assumption through CFD modeling and incorporating the effect of catalytic activity into the model description. Moreover, the implementation of the optimal design and the assessment of heat transfer capabilities represent key engineering challenges, whose resolution could be essential for scaling up and validating the proposed approach in real-world applications.

Data availability statement

The original contributions presented in the study are included in the article/supplementary material, further inquiries can be directed to the corresponding author.

Author contributions

DM: Conceptualization, Data curation, Formal Analysis, Investigation, Methodology, Software, Visualization, Writing – original draft. JQ-D: Formal Analysis, Visualization, Writing – original draft, Writing – review and editing. SK: Conceptualization, Formal Analysis, Methodology, Supervision, Writing – original draft, Writing – review and editing.

Funding

The author(s) declare that financial support was received for the research and/or publication of this article. SK is grateful to the Research Council of Norway for the Center of Excellence Funding Scheme, Grant No 262644, Porelab.

Conflict of interest

The authors declare that the research was conducted in the absence of any commercial or financial relationships that could be construed as a potential conflict of interest.

Generative AI statement

The author(s) declare that no Generative AI was used in the creation of this manuscript.

Publisher's note

References

Amhamed, A. I., Shuibul Qarnain, S., Hewlett, S., Sodiq, A., Abdellatif, Y., Isaifan, R. J., et al. (2022). Ammonia production plants—a review. *Fuels* 3, 408–435. doi:10.3390/fuels3030026

Baddour, R., Brian, P., Logeais, B., and Eymery, J. (1965). Steady-state simulation of an ammonia synthesis converter. *Chem. Eng. Sci.* 20, 281–292. doi:10.1016/0009-2509(65)85017-5

Bedeaux, D., Standaert, F., Hemmes, K., and Kjelstrup, S. (1999). Optimization of processes by equipartition. *J. Non-Equilibrium Thermodyn.* 24, 242–259. doi:10.1515/JNETDY.1999.015

Begall, M. J., Schweidtmann, A. M., Mhamdi, A., and Mitsos, A. (2023). Geometry optimization of a continuous millireactor via cfd and bayesian optimization. *Comput. and Chem. Eng.* 171, 108140. doi:10.1016/j.compchemeng.2023.108140

Biegler, L. (2010). *Nonlinear programming: concepts, algorithms, and applications to chemical processes*. Philadelphia: Society for Industrial and Applied Mathematics.

Bynum, M. L., Hackebeil, G. A., Hart, W. E., Laird, C. D., Nicholson, B. L., Siirola, J. D., et al. (2021). *Pyomo–optimization modeling in python*. 67. Springer Science and Business Media.

Chai, W. S., Bao, Y., Jin, P., Tang, G., and Zhou, L. (2021). A review on ammonia, ammonia-hydrogen and ammonia-methane fuels. *Renew. Sustain. Energy Rev.* 147, 111254. doi:10.1016/j.rser.2021.111254

Cheema, I. I., and Krewer, U. (2019). Optimisation of the autothermal nh3 production process for power-to-ammonia. *Processes* 8, 38. doi:10.3390/pr8010038

Chen, J., Shapiro, V., Suresh, K., and Tsukanov, I. (2007). Shape optimization with topological changes and parametric control. *Int. J. Numer. methods Eng.* 71, 313–346. doi:10.1002/nme.1943

Chonggen, P., Ying, L., Huazhang, L., and Liu, H. (2011). Effects of reaction conditions on performance of Ru catalyst and iron catalyst for ammonia synthesis. *Chin. J. Chem. Eng.* 19, 273–277. doi:10.1016/s1004-9541(11)60165-1

Courtais, A., Latifi, A. M., Lesage, F., and Privat, Y. (2021). Shape optimization of fixed-bed reactors in process engineering. *SIAM J. Appl. Math.* 81, 1141–1165. doi:10.1137/20m1343841

Courtais, A., Lesage, F., Privat, Y., Pelaingre, C., and Latifi, A. M. (2023). Cfd-based geometrical shape optimization of a packed-bed reactor combining multi-objective and adjoint system methods. *Chem. Eng. Sci.* 275, 118728. doi:10.1016/j.ces.2023.118728

El-Shafie, M., and Kambara, S. (2023). Recent advances in ammonia synthesis technologies: toward future zero carbon emissions. *Int. J. Hydrogen Energy* 48, 11237–11273. doi:10.1016/j.ijhydene.2022.09.061

Erfani, N., Baharudin, L., and Watson, M. (2024). Recent advances and intensifications in haber-bosch ammonia synthesis process. *Chem. Eng. Processing-Process Intensif.* 204, 109962. doi:10.1016/j.cep.2024.109962

Farsi, M., Chabi, N., and Rahimpour, M. (2021). Modeling and optimization of ammonia process: effect of hydrogen unit performance on the ammonia yield. *Int. J. Hydrogen Energy* 46, 39011–39022. doi:10.1016/j.ijhydene.2021.09.160

Flórez-Orrego, D., and de Oliveira Junior, S. (2017a). Exergy assessment of single and dual pressure industrial ammonia synthesis units. *Energy* 141, 2540–2558. doi:10.1016/j.energy.2017.06.139

Flórez-Orrego, D., and de Oliveira Junior, S. (2017b). Modeling and optimization of an industrial ammonia synthesis unit: an exergy approach. *Energy* 137, 234–250. doi:10.1016/j.energy.2017.06.157

Ghavam, S., Vahdati, M., Wilson, I., and Styring, P. (2021). Sustainable ammonia production processes. *Front. Energy Res.* 9, 580808. doi:10.3389/fenrg.2021.580808

Gillespie, L. J., and Beattie, J. A. (1930). The thermodynamic treatment of chemical equilibria in systems composed of real gases. I. An approximate equation for the mass action function applied to the existing data on the haber equilibrium. *Phys. Rev.* 36, 743–753. doi:10.1103/PhysRev.36.743

IEA (2021). *Ammonia technology road map*. France: International energy agency.

Johannessen, E., and Kjelstrup, S. (2004). Minimum entropy production in plug flow reactors: an optimal control problem solved for so_2 oxidation. *Energy* 29, 2403–2423. doi:10.1016/j.energy.2004.03.033

Kirova-Yordanova, Z. (2004). Exergy analysis of industrial ammonia synthesis. *Energy* 29, 2373–2384. doi:10.1016/j.energy.2004.03.036

Kizilova, N., Shankar, A., and Kjelstrup, S. (2024). A minimum entropy production approach to optimization of tubular chemical reactors with nature-inspired design. *Energies* 17, 432. doi:10.3390/en17020432

Kjelstrup, S., Bedeax, D., Johannessen, E., and Gross, J. (2010). *Non-equilibrium thermodynamics for engineers*. World Scientific.

Kojima, Y., and Yamaguchi, M. (2022). Ammonia as a hydrogen energy carrier. *Int. J. Hydrogen Energy* 47, 22832–22839. doi:10.1016/j.ijhydene.2022.05.096

Kumar, V. V., and Sharma, R. P. (2025). Entropy generation minimization in nuclear reactor cooling via rough rotating disk: a statistical approach. *Multiscale Multidiscip. Model. Exp. Des.* 8, 245. doi:10.1007/s41939-025-00846-8

Liu, H. (2014). Ammonia synthesis catalyst 100 years: Practice, enlightenment and challenge. *Chin. J. Catal.* 35, 1619–1640. doi:10.1016/S1872-2067(14)60118-2

Magnanelli, E., Solberg, S., and Kjelstrup, S. (2019). Nature-inspired geometrical design of a chemical reactor. *Chem. Eng. Res. Des.* 152, 20–29. doi:10.1016/j.cherd.2019.09.022

Mahapatra, S., and Dasappa, S. (2014). Influence of surface area to volume ratio of fuel particles on gasification process in a fixed bed. *Energy Sustain. Dev.* 19, 122–129. doi:10.1016/j.esd.2013.12.013

Månson, B., and Andresen, B. (1986). Optimal temperature profile for an ammonia reactor. *Ind. Eng. Chem. Process Des. Dev.* 25, 59–65. doi:10.1021/i200032a010

Meriño, F., Sauma, E., Manríquez, F., Pereira, A., and Vera, S. (2025). Long-term expansion planning of power systems considering renewable ammonia production under different scenarios for the year 2060. *Int. J. Hydrogen Energy* 127, 831–844. doi:10.1016/j.ijhydene.2025.03.290

Nadiri, S., Attari Moghaddam, A., Folke, J., Ruland, H., Shu, B., Fernandes, R., et al. (2024). Ammonia synthesis rate over a wide operating range: from experiments to validated kinetic models. *ChemCatChem* 16, e202400890. doi:10.1002/cctc.202400890

Nicholson, B., Siirola, J. D., Watson, J.-P., Zavala, V. M., and Biegler, L. T. (2017). pyomo.dae: a modeling and automatic discretization framework for optimization with differential and algebraic equations. *Math. Program. Comput.* 10, 187–223. doi:10.1007/s12532-017-0127-0

Nielsen, A., Kjaer, J., and Hansen, B. (1964). Rate equation and mechanism of ammonia synthesis at industrial conditions. *J. Catal.* 3, 68–79. doi:10.1016/0021-9517(64)90094-6

Nolasco, E., Vassiliadis, V. S., Kähm, W., Adloor, S. D., Ismaili, R. A., Conejeros, R., et al. (2021). Optimal control in chemical engineering: Past, present and future. *Comput. and Chem. Eng.* 155, 107528. doi:10.1016/j.compchemeng.2021.107528

Nummedal, L., Kjelstrup, S., and Costea, M. (2003). Minimizing the entropy production rate of an exothermic reactor with a constant heat-transfer coefficient: the ammonia reaction. *Ind. Eng. Chem. Res.* 42, 1044–1056. doi:10.1021/ie020319n

Ojelade, O. A., Zaman, S. F., and Ni, B.-J. (2023). Green ammonia production technologies: a review of practical progress. *J. Environ. Manag.* 342, 118348. doi:10.1016/j.jenvman.2023.118348

Penkuhn, M., and Tsatsaronis, G. (2017). Comparison of different ammonia synthesis loop configurations with the aid of advanced exergy analysis. *Energy* 137, 854–864. doi:10.1016/j.energy.2017.02.175

Poling, B. E., Prausnitz, J. M., and O'Connell, J. P. (2001). *The properties of gases and liquids*. McGraw-Hill.

Riera, J. A., Lima, R. M., and Knio, O. M. (2023). A review of hydrogen production and supply chain modeling and optimization. *Int. J. Hydrogen Energy* 48, 13731–13755. doi:10.1016/j.ijhydene.2022.12.242

Saffari, P. R., Salarian, H., Lohrasbi, A., and Salehi, G. (2021). Entropy generation analysis of a thermal cracking reactor. *ACS omega* 6, 6335–6347. doi:10.1021/acsomega.0c05937

Santoro, B. F., Rincón, D., and Mendoza, D. F. (2024). Entropy production and filling time in hydrogen refueling stations: an economic assessment. *Entropy* 26, 735. doi:10.3390/e26090735

Sauar, E., Nummedal, L., and Kjelstrup, S. (1999). The principle of equipartition of forces in chemical reactor design: the ammonia synthesis. *Comput. and Chem. Eng.* 23, S499–S502. doi:10.1016/S0098-1354(99)80123-9

Smith, C., Hill, A. K., and Torrente-Murciano, L. (2020). Current and future role of haber–bosch ammonia in a carbon-free energy landscape. *Energy and Environ. Sci.* 13, 331–344. doi:10.1039/c9ee02873k

Tondeur, D., and Kvaalen, E. (1987). Equipartition of entropy production. an optimality criterion for transfer and separation processes. *Industrial and Eng. Chem. Res.* 26, 50–56. doi:10.1021/ie00061a010

Xie, T., Xia, S., and Wang, C. (2022). Multi-objective optimization of braun-type exothermic reactor for ammonia synthesis. *Entropy* 24, 52. doi:10.3390/e24010052

Ye, D., and Tsang, S. C. E. (2023). Prospects and challenges of green ammonia synthesis. *Nat. Synth.* 2, 612–623. doi:10.1038/s44160-023-00321-7